HEP'99 # 7_116
Submitted to Pa 7
Pl 7, 8

DELPHI 99-72 CONF 259
15 June 1999

Search for non fermionic neutral Higgs couplings at LEP 2

Preliminary

DELPHI Collaboration

Paper submitted to the HEP'99 Conference
Tampere, Finland, July 15-21

Search for non fermionic neutral Higgs couplings at LEP 2

S. Andringa[1], M. Espírito Santo[2], P. Gonçalves[1], A. Onofre[1], R. Paiva[1], L. Peralta[1], M. Pimenta[1] and B. Tomé[1]

Abstract

Final states with isolated photons were explored in order to search for Higgs bosons with non fermionic couplings. The data collected by the DELPHI detector at a centre-of-mass energy of 189 GeV corresponding to an integrated luminosity of 153 pb^{-1} were analysed. No evidence for a signal was found and confidence limits were derived in the framework of possible extensions of the SM Higgs sector.

[1] LIP-IST-FCUL, Av. Elias Garcia, 14, 1, P-1000 Lisboa, Portugal

[2] CERN, CH1211 Geneva 23, Switzerland

1 Introduction

The Standard Model (SM) has been successful in describing the interactions between the gauge bosons and the fermions. Direct tests of the self-interactions of the electroweak gauge bosons are being carried out at LEP 2 and the Tevatron and no deviations from the SM have been observed so far. However, in the symmetry breaking sector there is no direct experimental evidence for the couplings of the gauge bosons to the Higgs boson. For this reason, many proposed extensions of the SM introducing changes in the Higgs sector are possible. This is in particular true for scenarios favoring non fermionic Higgs couplings. In this context, final states involving photons could constitute a rather distinctive signature.

In this paper non fermionic couplings are studied in two different frameworks. In one of them the SM Lagrangian is extended by introducing anomalous couplings of the Higgs boson to the vector bosons which lead in particular to direct H$\gamma\gamma$ and HZγ couplings [1]. A systematic exploration of this idea was recently done by DELPHI at $\sqrt{s} = 183$ GeV [2] and the present analysis can be considered as an update. In the second framework a Higgs sector with two doublets is considered, in the particular case of the fermiophobic scenario [3]. Most of the final state topologies are characterized in both frameworks by the presence of energetic and isolated photons. Limits on $\sigma(e^+e^- \to Hq\bar{q}) \times BR(H \to \gamma\gamma)$ from another LEP experiment can be found in reference [4].

The data were taken at a centre-of-mass energy of 189 GeV corresponding to an integrated luminosity of 153 pb^{-1}. A detailed description of the DELPHI detector and its performance can be found elsewhere [5, 6]. The effects of experimental resolution, both on the signals and on backgrounds, were studied by generating Monte Carlo events for the possible signals and for the SM processes and passing them through the full DELPHI simulation and reconstruction chain. The PYTHIA [7] generator was used to simulate the following process: $e^+e^- \to Z\gamma$, $e^+e^- \to WW$, $e^+e^- \to We\nu$, $e^+e^- \to ZZ$, and $e^+e^- \to Zee$. Bhabha events were generated with the Berends, Hollik and Kleiss generator [8], $e^+e^- \to \gamma\gamma\gamma$ events according to [9], and Compton events according to [10]. The two-photon ("$\gamma\gamma$") physics events were generated according to the TWOGAM [11] generator for quark channels and to the Berends, Daverveldt and Kleiss generator [12] for the Quark Parton Model giving hadrons.

2 Anomalous couplings

The production and decay rates of the Higgs boson could be enhanced by anomalous couplings to the vector bosons. These interactions can be expressed in terms of effective energy-dimension-six operators included in the interaction Lagrangian density [1, 2]:

$$\mathcal{L}_{eff} = \sum_{i=1}^{N} \frac{f_i}{\Lambda^2} O_i, \tag{1}$$

where the O_i are the operators which represent the anomalous couplings, Λ is the typical energy scale of the interaction and f_i are the constants which define the strength of each term. Six operators $f_{\phi,1}$, f_{BW}, f_B, f_W, f_{BB} and f_{WW} [1] give rise to the anomalous couplings H$\gamma\gamma$, HZγ, HZZ and HWW.

The most remarkable feature of this effective Lagrangian is the existence of direct HZγ and H$\gamma\gamma$ couplings, resulting in possible large deviations from the SM cross-sections of the studied processes. The production of the Higgs boson in association with photons would then increase and the decay $H \to \gamma\gamma$, which has a very small branching ratio in the SM, could even become dominant. A large enhancement of the $Z^* \to H\gamma$ decay width would imply coefficients $\frac{f_i}{\Lambda^2}$ of the order of $10 - 100$ TeV^{-2}.

On the other hand, the introduction of $\mathcal{L}_{eff}$ (equation 1) as an extension to the SM Lagrangian would also contribute to other processes besides the Higgs boson interactions, namely to gauge boson self-interactions Therefore, some of the $\frac{f_i}{\Lambda^2}$ coefficients, namely $f_{\phi,1}$ and f_{BW}, are already bound by precise measurements of the SM parameters [13]. In what follows, the $f_{\phi,1}$ and f_{BW} coefficients will be taken as zero, and only f_B, f_W, f_{BB} and f_{WW} will be considered.

The Higgs boson production and decay processes where anomalous HZγ, HZZ and H$\gamma\gamma$ couplings are present at tree level are displayed in figure 1. However, processes 1(e) and 1(f) will not be taken into account in the analyses, since they are expected to be negligible in most of the parameter space. Table 1 summarizes the studied processes, the final state topologies and the relevant mass regions. The region below the lower mass constraint is excluded by the standard Higgs searches.

Signals events were simulated using the PYTHIA generator [7]. Higgs boson masses (m_H), ranging from 80 to 170 GeV/c^2 were considered.

The interpretation of the results requires the computation of the cross-sections as a function of the anomalous couplings, f_i/Λ^2, as well as of m_H. The CompHEP package was used for this calculation [14]. All the new interactions were incorporated in the generator using the LanHEP code [15]. In a scenario where the anomalous contributions to the cross-section are important, the Higgs boson width depends on the f_i values and must be supplied to CompHEP. The computation of the Higgs boson width was taken from [1] and [16] and includes the interference between the SM model contribution and the new anomalous diagrams. In the studied m_H range decays of the Higgs boson into ZZ* or WW* are important [17] and their contribution was taken into account. The Higgs boson width increases for higher values of the Higgs mass and for increasing absolute values of the anomalous couplings. It ranges from a few MeV up to hundreds of MeV, never reaching the experimental resolution for the range of masses and couplings considered.

Process	Final State	Relevant mass region (GeV)
$e^+e^- \to H\gamma$	$\gamma\gamma\gamma$	$80 < m_H < 170$
	$b\bar{b}\gamma$	
$e^+e^- \to HZ$	$\gamma\gamma\nu\nu$	$80 < m_H < 100$
$e^+e^- \to HZ/\gamma^*$	$\gamma\gamma q\bar{q}$	$80 < m_H < 170$

Table 1: Observable topologies corresponding to the different final states in the framework of the anomalous couplings model.

3 2HDM: A fermiophobic scenario

The two Higgs Doublets Models (2HDM) without explicit CP violation [3] are characterized by seven parameters corresponding to five physical Higgs bosons: two neutral CP-even bosons (h^0, H^0), two charged bosons ($H^{\pm}$), and one neutral CP-odd boson (A^0). The free parameters are usually chosen as the four Higgs masses and the angles α and β, where $tan\ \beta$ represents the ratio of the vacuum expectation values of the two Higgs doublets and α the mixing angle of the neutral CP-even Higgs sector. The seventh parameter is related to the masses of the vector bosons Z and W which are nowadays extremely well measured [18].

In the framework of 2HDM there are four different ways in which the Higgs doublets can couple to fermions [19]. The most common choice is the structure assumed in the Minimal SuperSymmetric Model [20] : one of the Higgs doublets couples both to up type quarks and to leptons, and the other doublet couples to down type quarks. In this paper a model of the so called type I is explored, i.e. only one of the Higgs doublet is allowed to couple to fermions. The coupling of the lightest CP-even boson h^0 to a fermion pair is then proportional to $cos\ \alpha$. If $\alpha = \frac{\pi}{2}$ this coupling vanishes and h^0 becomes a fermiophobic Higgs.

The Higgs-Higgs interactions, namely the $h^0H^+H^-$ vertex, depend on the specific 2HDM potential. In fact there are two different seven parameter potentials, referred to as potential A and potential B [3], both assuring no explicit CP violation. These potentials are equivalent in what concerns the Higgs coupling to gauge bosons and fermions. However, differences in the Higgs-Higgs interactions leads to different phenomenologies and to different forbidden regions in the parameter space accessible at LEP.

3.1 Production and decay of the h^0 and A^0 bosons

In the 2HDM the main mechanisms for the production of neutral Higgs bosons are $e^+e^- \rightarrow hZ^*$ and $e^+e^- \rightarrow hA$. These processes have complementary cross-sections, proportional to $sin^2\delta$ and to $cos^2\delta$ respectively, where $\delta = \alpha - \beta$. The relevant diagrams are displayed in figure 2 and the cross-sections values at $\sqrt{s} = 189$ GeV are illustrated in figure 3 as function of the masses.

The dominant decay modes for $m_h < m_Z$ in the considered fermiophobic limit (Model I and $\alpha = \frac{\pi}{2}$) are $h^0 \rightarrow A^0A^0$ (tree level) if $m_{h^0} > 2m_{A^0}$ and $h^0 \rightarrow \gamma\gamma$ (one-loop) otherwise [3]. The h^0 decays to a pair of massive vector bosons are suppressed by a $sin^2\delta$ factor, but can be important when $m_h > m_Z$. The one loop decay $h \rightarrow Z\gamma$ is never dominant but its branching ratio can be, in specific parameter regions ($m_h > m_Z$ and very small δ values) as large as 20%. Considering the present limits on $m_{H^{\pm}}$ [21], the h^0 decays into charged Higgs bosons are hardly accessible at LEP.

The tree level decay modes of the A^0 boson are : $A^0 \rightarrow f\overline{f}$, $A^0 \rightarrow Zh^0$, and $A^0 \rightarrow W^{\pm}H^{\pm}$. The decay involving the charged Higgs boson is not considered in this analysis due, once again, to the the present limit on $m_{H^{\pm}}$ and the available LEP energy and luminosity. Above the Zh^0 threshold the decay $A^0 \rightarrow Zh^0$ is dominant for all the interesting region of δ ($\delta < 0.5$). Below the Zh^0 threshold A^0 decays mainly into a fermion-antifermion pair, namely a $b\overline{b}$ pair when $m_{A^0} > 10$ GeV. Finally it should be noted that in the region of very low δ values ($\delta < 10^{-3}$) and $m_{A^0} < m_Z + m_{h^0}$ the A^0 total width is very small and A^0 can leave the detector before decaying [3].

All the processes, but the associated h^0A^0 production with $h^0 \to A^0A^0$, are characterized by the presence of isolated and energetic photons.

3.2 Relevant parameter space regions

The study at LEP2 of the final topologies discussed above can explore a relevant fraction of the allowed parameter space of the 2HDM fermiophobic scenario. The high δ region can be studied analyzing the Higgs-strahlung process while the small δ region is constrained by the associate production. The combination of both process leads to an interpretation of the results as a function of m_{h^0} and m_{A^0}.

The region in the plane (m_{h^0}, m_{A^0}) that is relevant for the present analysis corresponds to a band $m_{low} < m_{A^0} + m_{h^0} < m_{high}$. The upper constraint ($m_{high} <\sim 160$ GeV) represents the sensitivity accessible with the present luminosity and energy of LEP2, and the lower constrain ($m_{low} >\sim 40$ GeV) indicates the region excluded by previous analyses namely at LEP1. while for potential B it corresponds to $m_h^0 \sim m_A^0$ [3].

The several topologies contributing to this analysis are summarized in table 2. In the case of the $b\bar{b}b\bar{b}b\bar{b}$ final state the analysis of reference [22] is used.

Process	Final states	Relevant mass region (GeV)
$e^+e^- \to h^0A^0$	$\gamma\gamma A^0$(long lived)	$m_A < m_Z + m_h$
	$\gamma(\gamma)b\bar{b}$	$m_h + m_A > 40$
$e^+e^- \to h^0A^0 \to h^0h^0Z$	$\gamma\gamma\gamma\gamma\nu\nu$	$m_A > m_Z + m_h$
	$\gamma\gamma\gamma\gamma q\bar{q}$	
$e^+e^- \to h^0A^0 \to A^0A^0A^0$	bbbbbb	$m_h > 2m_A$
$e^+e^- \to h^0Z$	$\gamma\gamma\nu\bar{\nu}$	$10 < m_h < 100$
	$\gamma\gamma q\bar{q}$	

Table 2: Observable topologies corresponding to the different final states in the framework of the 2HDM.

4 Event selection

Charged particles were considered only if they had momentum greater than 0.1 GeV/c and impact parameters below 4 cm in the transverse plane and 4/sinθ cm in the beam direction.

Neutral clusters above 2 GeV were classified as isolated photons if the total energy inside a double cone centered around the cluster with half angles of 5° and 15°, was less than 1 GeV and if there were no charged particles above 0.25 GeV/c inside the inner cone. The energy of the isolated photons was then reevaluated as the sum of the energies of all the particles inside the inner cone.

The algorithm used to identify isolated charged particles demanded that inside a double cone centered on the track, with internal and external half angles of 5° and 25°, the total charged energy was less than 1 GeV and the total neutral energy was less than 2

GeV. The energy of the particle was redefined as the sum of the energies of all the charged and neutral particles inside the inner cone and required to be greater than 4 GeV.

For the topologies with just photons in the final state, the visible energy in the polar angle region between 20° and 160° was required to be above 0.1 $\sqrt{s}$, and the minimum energy of each photon was required to be 3 GeV. Whenever more than 3 GeV of hadronic energy was associated to a photon, at least 90 % of it had to be in the first layer of the Hadronic Calorimeter (HCAL).

Hadronic topologies required that at least six charged tracks were present as well as visible energy in the polar angle region between 20° and 160° above 0.2 $\sqrt{s}$ including at least one charged particle with an energy greater than 5 GeV, and at least one electromagnetic cluster with energy greater than 5 GeV. No isolated charged particles were allowed. A protection against fake photons was set by requiring less than 1 GeV in the HCAL and no High Density Projection Chamber (HPC) layer with more than 90% of the photon electromagnetic energy. Alternatively an energy deposition in the hadronic calorimeter was allowed if at least 90% was in the first layer.

All selected charged particles and neutrals not associated to photons were forced to be clustered into two jets using the DURHAM jet algorithm [23].

4.1 Photonic final states

Selection criteria were implemented to identify events with two or more isolated photons.

The non-converted photons had to fulfill the following requirements:

- no charged tracks could be associated to the energy deposit. Moreover, no Vertex Detector (VD) track element could point to the photon within 3° (10°) in azimuthal angle in the barrel (forward) region of DELPHI (a VD track element was defined as at least two hits in different VD layers aligned within an azimuthal angle interval of 0.5°).

- Photons candidates were required to have energies above 5 GeV and to be isolated by at least 30°.

- If the photon candidate was located inside the FEMC (Forward ElectroMagnetic Calorimeter) its polar angle had to be greater than 25° (145°) and less than 35° (155°);

- If the photon candidate was inside the HPC then :

  - Its polar angle had to be greater than 42° and less than 88° or greater than 92° and less than 138°;
  - If its azimuthal angle lay outside the inter-modular divisions [1], there had to be at least three HPC layers with more than 5% of the total electromagnetic energy of the photon candidate.

Photons converting after the VD in the polar angle range between 25° and 155° were recovered. Charged jets containing up to five charged tracks associated to energy deposits

[1] $\mathrm{mod}(\phi, 15°) = 7.5° \pm 1.0°$, for more details see [5, 6]

above 3 GeV were considered as photon conversions if their signature in the electromagnetic (and hadronic) calorimeters fulfilled the selection criteria described above.

The preselected sample (level 1) consisted of events with at least two photons fulfilling the above criteria. Specific criteria were implemented accordingly to the final state topology.

4.1.1 Two acoplanar photons events

The $\gamma\gamma$ acoplanar sample consisted of events with two and only two photons fulfilling the following conditions (level 2):

- Whenever the missing momentum was greater than 0.1 $\sqrt{s}$ the polar angle of the direction of the missing momentum was required to be greater than 10° and no signal in the set of lead/scintillator counters placed between the barrel and forward electromagnetic calorimeters was allowed.

- One photon was allowed to be converted.

The final selection criterion (level 3) consisted of imposing that the acoplanarity was greater then 10° and the total energy lower than 0.7 $\sqrt{s}$.

4.1.2 Three photon events

The $\gamma\gamma\gamma$ sample preselection consisted on selecting events with two or more photons fulfilling the following conditions (level 2):

- The two most energetic photons were required to have energies above 15% of the collision energy.

- One photon was allowed to be converted.

The final selection criterion (level 3) consisted on requiring that there were three photons in the event and that the less energetic photon had an energy above 6% of the collision energy and that is was isolated by at least 15° from other particles. Moreover, the events were required to be planar: it was required that the sum of the spatial angles between the photons was above 350°. A three body kinematical fit was then applied to the events, according to momenta and energy conservation, given the good spatial resolution of the DELPHI electromagnetic calorimeters. The compatibility of the momenta calculated from the angles with the measured momenta was quantified on a χ^2 basis [2]. The χ^2 variable resulting from the kinematical fit was required to be below 3. The invariant masses of the photon pairs were reevaluated using the fitted energy values.

[2]The χ^2 parameter was defined as $\chi^2 = \frac{1}{3}\sum_{i=1,3}\left(\frac{p_i^{calc}-p_i^{meas}}{\sigma_i}\right)^2$ p_i^{meas} are the measured momenta or energies and p_i^{calc} are the momenta calculated from the kinematic constraints. σ_i, is defined in reference [24] for the three photon topology.

4.1.3 Four photon events

The $\gamma\gamma\gamma\gamma$ sample consisted of events with at least two photons fulfilling the following conditions (level 2):

- Whenever the missing momentum was greater than 0.1 $\sqrt{s}$ the polar angle of the direction of the missing momentum was required to be greater than 10° and no signal in the set of lead/scintillator counters placed between the barrel and forward electromagnetic calorimeters was allowed.
- One photon was allowed to be converted.

The final selection criterion (level 3) consisted of imposing that the acoplanarity between the two most energetic photons was greater then 10° and the missing energy greater than 70 GeV.

4.2 Final states with jets and photons

Selection criteria were implemented to identify events with two jets and at least one isolated photon (level 1).

For $b\overline{b}\gamma$, $q\overline{q}\gamma\gamma$ or $b\overline{b}\gamma\gamma$ and $q\overline{q}\gamma\gamma\gamma\gamma$ final states one, two and three photons with polar angle above 40° were required respectively. Moreover for $b\overline{b}\gamma$ the photon energy was asked to be greater than 10 GeV.

In order to improve momentum and energy resolution, a kinematic fit [25] imposing total energy and momentum conservation was performed on the selected events with one or two isolated photons. Only events with a χ^2 per degree of freedom lower than 5 were accepted.

After these cuts (level 2), whenever the main decay channel for the Higgs bosons h^0 or A^0 is through $b\bar{b}$ event flavour tagging was performed based on the identification of the final state quark. Events with a high probability of containing a b quark (b-tag variable, as defined in references [6] and [26], greater than -2) were thus accepted (level 3).

5 Results

The number of candidates at different selections levels for the relevant topologies are given in table 3. The numbers in brackets give the Standard Model expectations. In the different selection levels and topologies, fair agreement between data and MC expectations is found and therefore no evidence for unexpected phenomena can be claimed.

The efficiencies, including the trigger efficiency, were calculated for each final state topology according to the the specific process to be studied (see sections 2 and 3) at several mass points covering the relevant parameter phase space. The values shown in the last column of table 3 are averages values.

Model-independent limits at 95% Confidence Level (CL) on the cross-sections were derived for the different processes studied as a function of the Higgs boson masses and branching ratios. The limits were obtained using a Poisson distribution with background [27] and taking into account, when available, the mass resolution information for each topology. The 95% CL upper limits on the cross-section for the HZ/γ^* and $H\gamma$ are displayed in figure 4. Figure 5 shows the limits for h^0A^0 associated production.

topology	selection level 1	selection level 2	selection level 3	Efficiency (%)
$\gamma\gamma\gamma\gamma$	1733 (1678±7)	709 (680±4)	7 (5.6±0.5)	30
$\gamma\gamma\gamma$	1733 (1678±7)	797 (651±4)	9 (11.7±0.6)	35
$\gamma\gamma$	1733 (1678±7)	628 (614±4)	8 (3.8±0.5)	50
$b\bar{b}\gamma$	3164 (3097±31)	395 (449±11)	168 (202±8)	50
$q\bar{q}\gamma\gamma$	226 (230±8)	21 (15±2)		30
$b\bar{b}\gamma\gamma$	226 (230±8)	21 (15±2)	10 (6±1)	26
$q\bar{q}\gamma\gamma\gamma\gamma$	11 (10±1)	1 (0.3±0.3)		30

Table 3: Number of events passing the sets of cuts corresponding to the selection levels described in the text for each topology and centre-of-mass energy. The MC predicted numbers of events and their statistical errors, are displayed within parentheses. Selection level 3 applies only to the $b\bar{b}\gamma$ and $b\bar{b}\gamma\gamma$ topologies. The efficiencies shown in the last column are average values.

6 Limits on anomalous couplings

Limits on the anomalous couplings were computed for a centre-of-mass energy of 189 GeV. They were set assuming three different scenarios:

In the first scenario each f_i parameter was considered independently by setting all the others to zero. Limits on each f_i/Λ^2 parameter were set as a function of the Higgs boson's mass (figure 6). The $\gamma\gamma\gamma$ analysis contributes to set exclusion limits on the values of $|f_{BB}/\Lambda^2|$ and $|f_{WW}/\Lambda^2|$ for Higgs boson masses up to 160 GeV/c^2. The $q\bar{q}\gamma\gamma$ analysis excludes additional values of f_{BB} and f_{WW} for masses m_H up to 85 GeV/c^2 and 95 GeV/c^2, respectively. The $b\bar{b}\gamma$ cross-section has a weak dependence on f_{BB} and f_{WW} and the analysis of this process does not improve the limits on these two parameters.

When f_{BB} and f_{WW} are zero, $H \to \gamma\gamma$ has a negligible rate so the $\gamma\gamma\gamma$ and $Z^0\gamma\gamma$ processes do not contribute to set limits on other parameters. In this case $H \to b\bar{b}$ is the dominant decay and limits on f_B and f_W may be obtained for m_H up to 120 GeV/c^2 (figures 6 (c) and (d)).

Also shown in figure 6 (c) are the limits obtained on the anomalous TGC parameters by the direct measurements of WW production [28] (horizontal lines), f_B/Λ^2 and f_W/Λ^2 contribute also to the TGCs, and the resulting constraints from the $b\bar{b}\gamma$ analysis give indirect limits on the deviations from the SM trilinear gauge boson couplings vertices. The anomalous $WW\gamma$ and WWZ dipole like couplings and the WWZ charge like couplings are defined as:

$$\Delta k_\gamma = \frac{m_W^2}{2}\frac{(f_B + f_W)}{\Lambda^2}, \qquad \Delta k_Z = \frac{m_W^2}{2}\frac{(f_B.\tan^2\theta_W + f_W)}{\Lambda^2}, \qquad \Delta g_1^Z = \frac{m_Z^2}{2}\frac{f_W}{\Lambda^2} \tag{2}$$

In the case in which only f_B is different from zero, Δk_γ is proportional to f_B/Λ^2 and Δg_1^Z is zero, assumptions used in the TGC direct limit for Δk_γ. In this case the limit

obtained with the $b\bar{b}\gamma$ analysis improves the direct limit for m_H up to 120 GeV/c^2.

In the second scenario, all f_i except f_{BB} and f_{WW} (which directly contribute to the decay H $\rightarrow \gamma\gamma$) were assumed to be negligible. In this scenario, the derived 95% CL cross-section upper limits were used to exclude regions in the f_{WW} vs f_{BB} plane. The contour plots of the limits obtained from the b$\bar{\text{b}}\gamma$, q$\bar{\text{q}}\gamma\gamma$ and $\gamma\gamma\gamma$ analyses are displayed in figure 7 for $m_H = 100$ GeV/c^2. Each final state contributes to exclude particular regions in the f_{WW} vs f_{BB} plane.

In the third scenario the simplest assumption was made. All f_i's have a strength of the same order and are set to $f_i = F$. The $Z\gamma\gamma$ cross-section shows a clear asymmetry between positive and negative values of F/Λ^2, due to the interference between the anomalous and standard HZZ coupling (figure 1(c)). For the other final states there is no such interference, as in the SM there is no tree-level vertex for the Higgs boson production with a photon.

In this scenario, limits on F/Λ^2 as a function of the Higgs boson mass were derived (figure 8). Constraints on F/Λ^2 from the $\gamma\gamma\gamma$ analysis results are of the order $\pm$ 25 TeV^{-2} for $m_H < 100$ GeV/c^2 and $\pm$ 50 TeV^{-2} up to 160 GeV/c^2. The q$\bar{\text{q}}\gamma\gamma$ and $\nu\bar{\nu}\gamma\gamma$ analyses results set limits for m_H up to 120 GeV/c^2 and 110 GeV/c^2, respectively. This is due to the fact that the Z$\gamma\gamma$ cross-section decreases above $m_H = 100$ GeV/c^2 (corresponding to the kinematic limit for HZ production). The Z$\gamma\gamma$ contributions improve slightly the $\gamma\gamma\gamma$ limit on negative F values for $m_H < 96$ GeV/c^2. For the case of positive F values, the interference between anomalous and SM HZZ couplings is destructive and the limit from $\gamma\gamma\gamma$ remains unchanged. In the considered mass region, the result from the b$\bar{\text{b}}\gamma$ analysis does not improve the previous limits.

7 Limits on fermiophobic Higgs boson production

The interpretation of the results presented in section 5 in terms of expected cross-sections discussed in section 3 leads to exclusion regions in the parameter space of the model.

The 95 % CL limits in the plane (m_{h^0}, $sin^2\delta$), obtained directly from the Higgs-strahlung final states, assuming $h^0 \rightarrow \gamma\gamma$, are shown in figure 9. When $\delta \rightarrow 0$ the Higgs-strahlung cross-section vanishes and no limit on m_{h^0} can be set. For $sin^2\delta = 1$, m_{h^0} is excluded up to 96 GeV/c^2.

The number of expected events for each pair of values (m_{h^0}, m_{A^0}) is given by the sum of the contributions from the h^0Z and h^0A^0 channels which are proportional to $sin^2\delta$ and $cos^2\delta$ respectively. Whenever for any value of δ the confidence level computed with this expected number of events is greater than 95 %, the corresponding point in the plane (m_{h^0},m_{A^0}) is excluded. The limits thus obtained are shown in figure 10. Branching ratios equal to 1 were assumed for the dominant decay channel in each mass region. The dark region corresponds to the decay modes $h^0 \rightarrow \gamma\gamma$ and $A^0 \rightarrow b\bar{b}$ or A^0 long-lived. The light region was taken from reference [22] and corresponds to $h^0 \rightarrow A^0A^0$ and $A^0 \rightarrow b\bar{b}$.

8 Conclusions

DELPHI data corresponding to an integrated luminosity of 153 pb^{-1}, at the centre-of-mass energy of 189 GeV, have been analysed and a search for neutral Higgs boson with important non fermionic couplings was performed. The final states $\gamma\gamma$, $\gamma\gamma\gamma$, $\gamma\gamma\gamma\gamma$, b$\bar{\text{b}}\gamma$, b$\bar{\text{b}}\gamma\gamma$, q$\bar{\text{q}}\gamma\gamma$, q$\bar{\text{q}}\gamma\gamma\gamma\gamma$ were considered. No evidence for unexpected phenomena has been

found. Upper limits on the cross-sections of these processes were derived at 95 % CL as a function of the Higgs masses. The cross-section upper limits were interpreted in two different frameworks. Limits on contributions from operators which could give rise to anomalous Higgs to gauge boson couplings and trilinear gauge boson couplings were derived. A large region of the parameter space in a 2HDM fermiophobic scenario was excluded.

Acknowledgements

We would like to thank L.Brücher and R.Santos for very interesting and long discussions in exploring the 2HDM fermiophobic scenario.

We are greatly indebted to our technical collaborators, to the members of the CERN-SL Division for the excellent performance of the LEP collider, and to the funding agencies for their support in building and operating the DELPHI detector.

References

[1] K. Hagiwara, R. Szalapski, D. Zeppenfeld, Phys. Lett. **B318** (1993) 155

[2] DELPHI Coll., P. Abreu et al., "Search for the Higgs boson in events with isolated photons at LEP II", to be submitted to Physics Letters B

[3] A. Barroso, L. Brücher, R. Santos, "Is there a light fermiophobic Higgs?", hep-ph/9901293

L. Brücher, R. Santos, "Experimental signatures of fermiophobic Higgs" in preparation

[4] OPAL Coll.,K. Ackerstaff et al., Phys. Lett. **B437** (1998) 218

[5] DELPHI Coll., P. Aarnio et al., Nucl. Instr. and Meth. **A303** (1991) 233

[6] DELPHI Coll., P. Abreu et al., Nucl. Instr. and Meth. **A378** (1996) 57

[7] T. Sjöstrand, Comp. Phys. Comm. **82** (1994) 74,

T. Sjöstrand, Pythia 5.7 and Jetset 7.4, Cern-TH/7112-93

[8] F.A. Berends, W. Hollik and R. Kleiss, Nucl. Phys. **B304** (1988) 712

[9] F. Berends and R. Kleiss, Nucl. Phys. **B186** (1981) 22

[10] D. Karlen, Nucl. Phys. **B289** (1987) 23

[11] S. Nova, A. Olchevski and T. Todorov, "TWOGAM, a Monte Carlo event generator for two photon physics", DELPHI Note 90-35 PROG 152

[12] F.A. Berends, P.H. Daverveldt, R. Kleiss, Comp. Phys. Comm. **40** (1986) 271

[13] K. Hagiwara, S. Ishihara, R. Szalapski, D. Zeppenfeld, Phys. Rev. **D48** (1993) 2182

S. Andringa, "Standard and Anomalous Final States with Photons at LEP2: QED bremsstrahlung and Anomalous Decays of the Higgs", Master Thesis, Lisboa 1999

[14] E.E. Boos, M.N. Dubinin, V.A. Ilyin, A.E. Pukhov, V.I. Savrin, Preprint INP MSU 94-36/358 and SNUCTP 94-116 (1994); hep-ph/9503280,

P.A. Baikov et al., in Proc. X Workshop QFTHEP-95 (Zvenigorod, September 1995), ed. B. Levtchenko and V. Savrin (MSU, Moscow, 1996) p.101; hep-ph/9701412

[15] A.V. Semenov, "LanHEP- a package for automatic generation of Feynman rules in gauge models", INP-MSU-96-24-431 and hep-ph/9608488

[16] J.C. Romão and S. Andringa, "Vector Boson Decays of the Higgs", hep-ph/9807536

[17] A. Djouadi,"Decays of the Higgs boson", hep-ph/9712334

[18] LEP and SLD Coll. "A Combination of Preliminary Electroweak Measurements and Constraints on the Standard Model"CERN-EP/99-015

[19] A G Akeroyd, "Three-body decays of Higgs bosons at LEP2 and application to a hidden fermiophobic Higgs", (hep-ph/9806337

J.F. Gunion, H.E.Haber, G.L.Kane and S. Dawnson, "The Higgs Hunter's Guide" (Addison-Wesley, Reading 1990)

[20] See for example:

H.P.Nilles, Phys. Rep.**110** (1984)1

M.E.Haber and G.L.Kane, Phys. Rep. **117**(1985)75

M.F.Sohnius, Phys. Rep. **128**(1985)39

[21] LEP Coll. "Limits on Higgs boson masses from combining the data of the four LEP experiments at $\sqrt{s} \leq 183$ GeV", CERN-EP/99-060

ALEPH Coll. R. Barate et al. , Phys. Lett., **B450** (1999) 467

DELPHI Coll., "search for Charged Higgs Bosons at Lep2", Delphi 98-96 CONF164

L3 Collaboration. H. Acciarri et al, Phys. Lett., **B446** (1999) 368

OPAL Coll. G. Abbiendi et al. , Eur. Phys. J., **C7** (1999) 407

[22] DELPHI Coll. "Interpretation of the search for Neutral Higgs Bosons in two-Doublet Models", Delphi-98-117 CONF 179

[23] S. Catani et al., Phys. Lett. **B269** (1991) 432

[24] DELPHI Coll., P. Abreu et al., Phys. Lett. **B380** (1996) 480,

DELPHI Coll., P. Abreu et al., Zeit. Phys. **C53** (1992) 41

[25] DELPHI Coll., P. Abreu et al., Eur. Phys. J. **C2** (1998) 581

[26] G. Borisov and C. Mariotti, "Performance of b-tagging at LEP2",DELPHI 97-16 PHYS 672

[27] Particle Data Group, R. M. Barnett et al., Phys.Rev. **D54** (1996) 1

[28] T.J.V. Bowcock et al., "Measurement of Trilinear Gauge Boson Couplings WWV (V $\equiv \gamma, Z$) in e^+e^- Collisions at 183 GeV", DELPHI 98-94 CONF 162

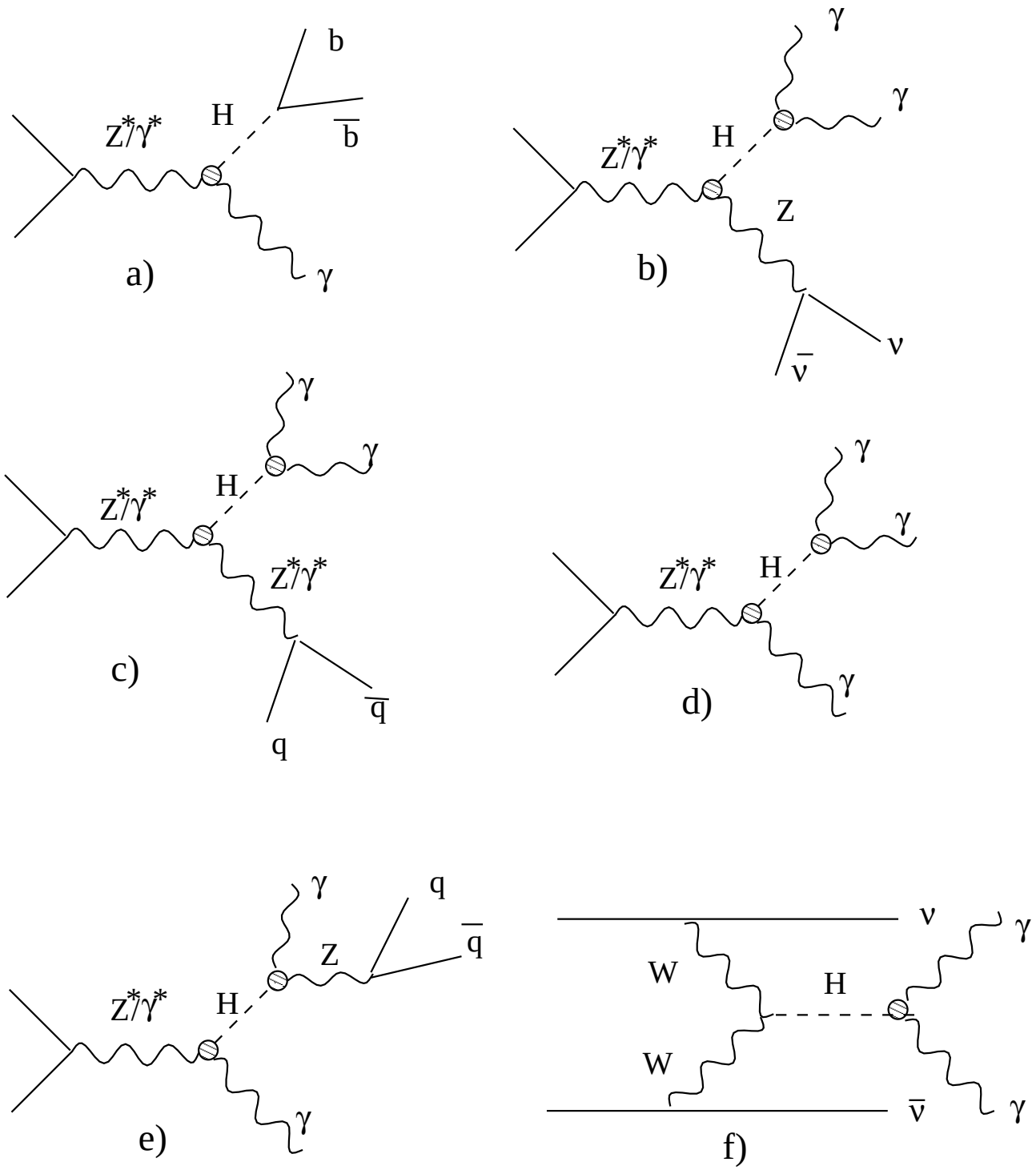

Figure 1: Feynman diagrams for the anomalous Higgs production at LEP.

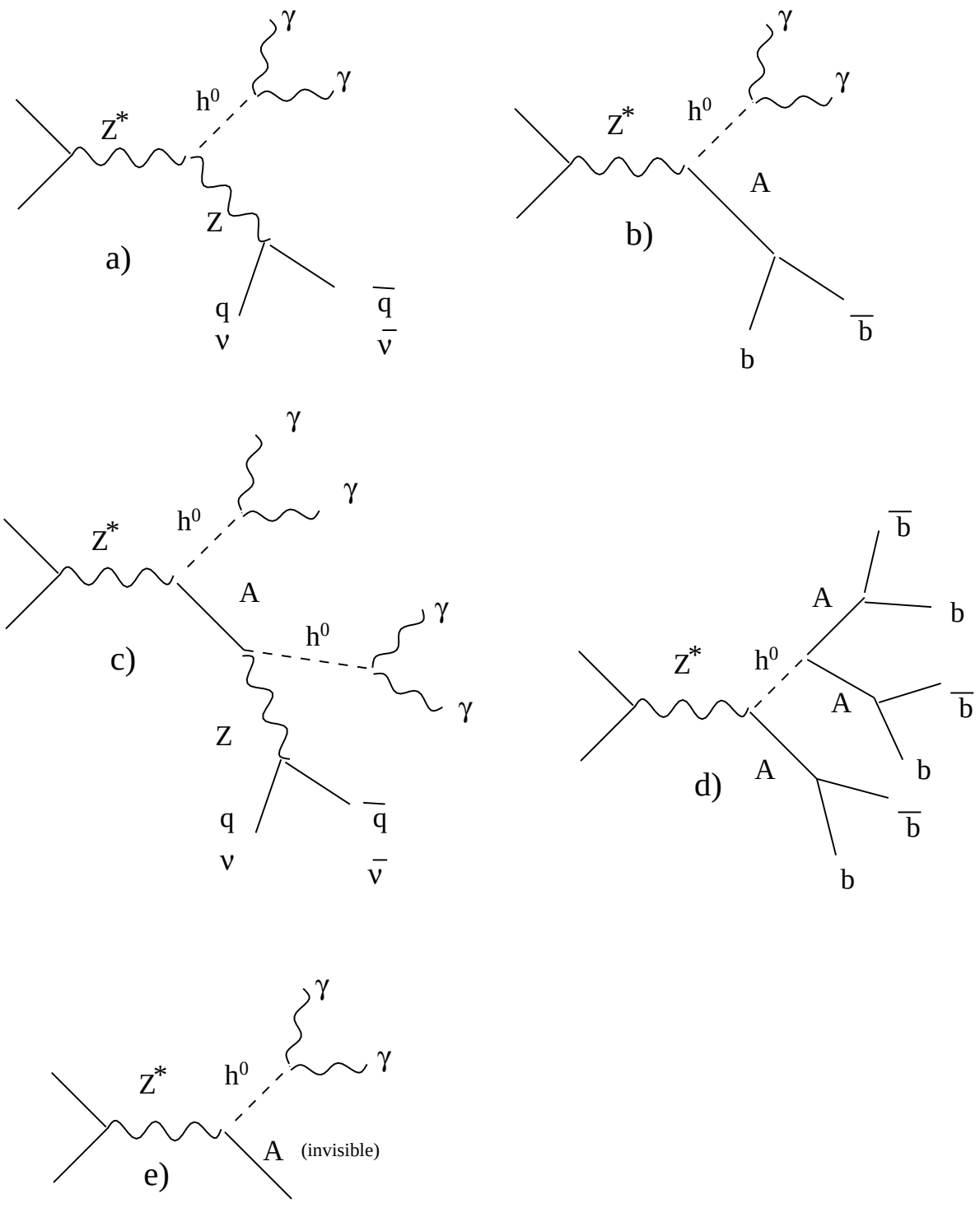

Figure 2: Feynman diagrams for h^0 production in the 2HDM model at LEP.

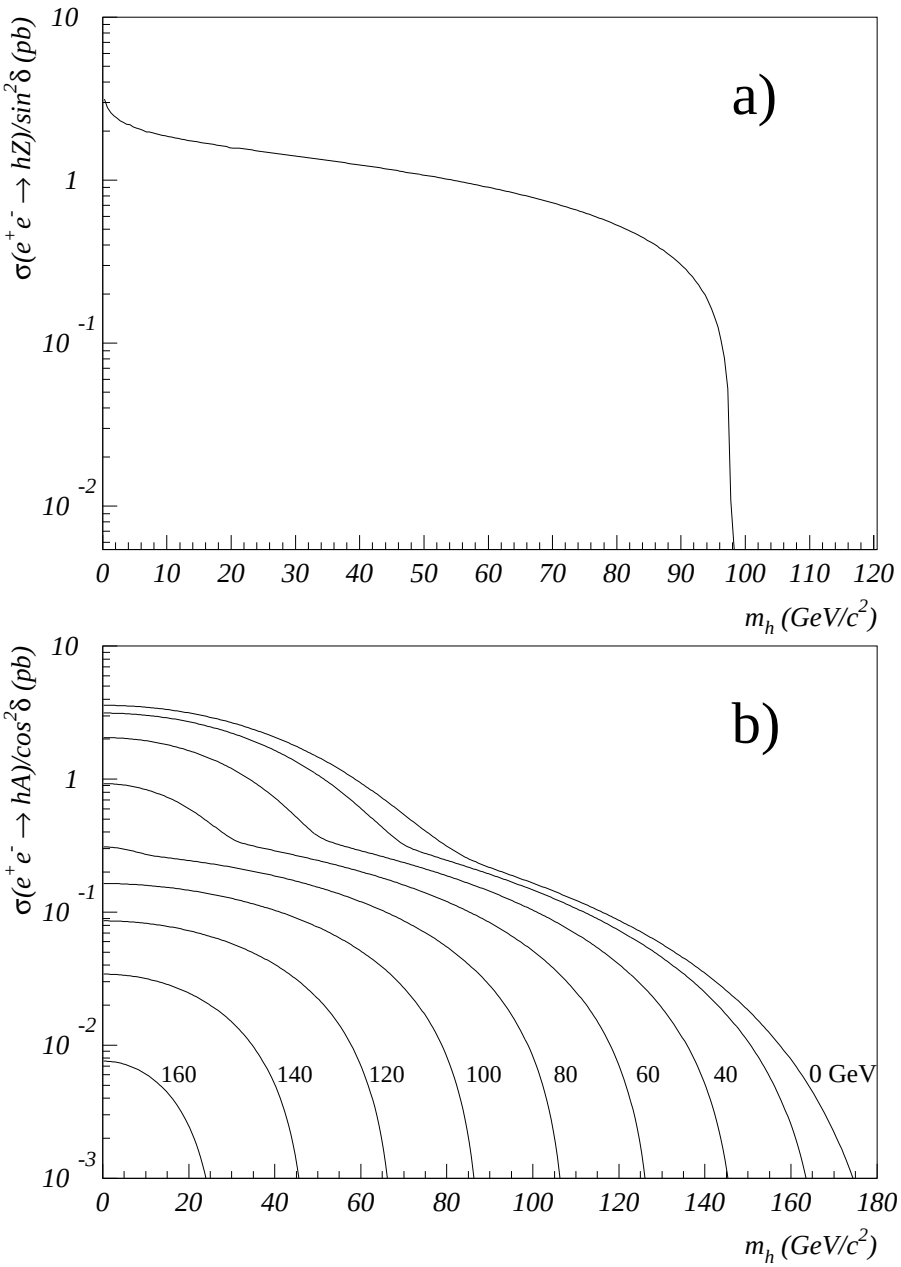

Figure 3: Cross-section for: a) the Higg-strahlung production b) h^0A associated production. The successive lines in b) correspond to m_A values from 0 (outer line) to 160 GeV/c^2 in 20 GeV/c^2 steps.

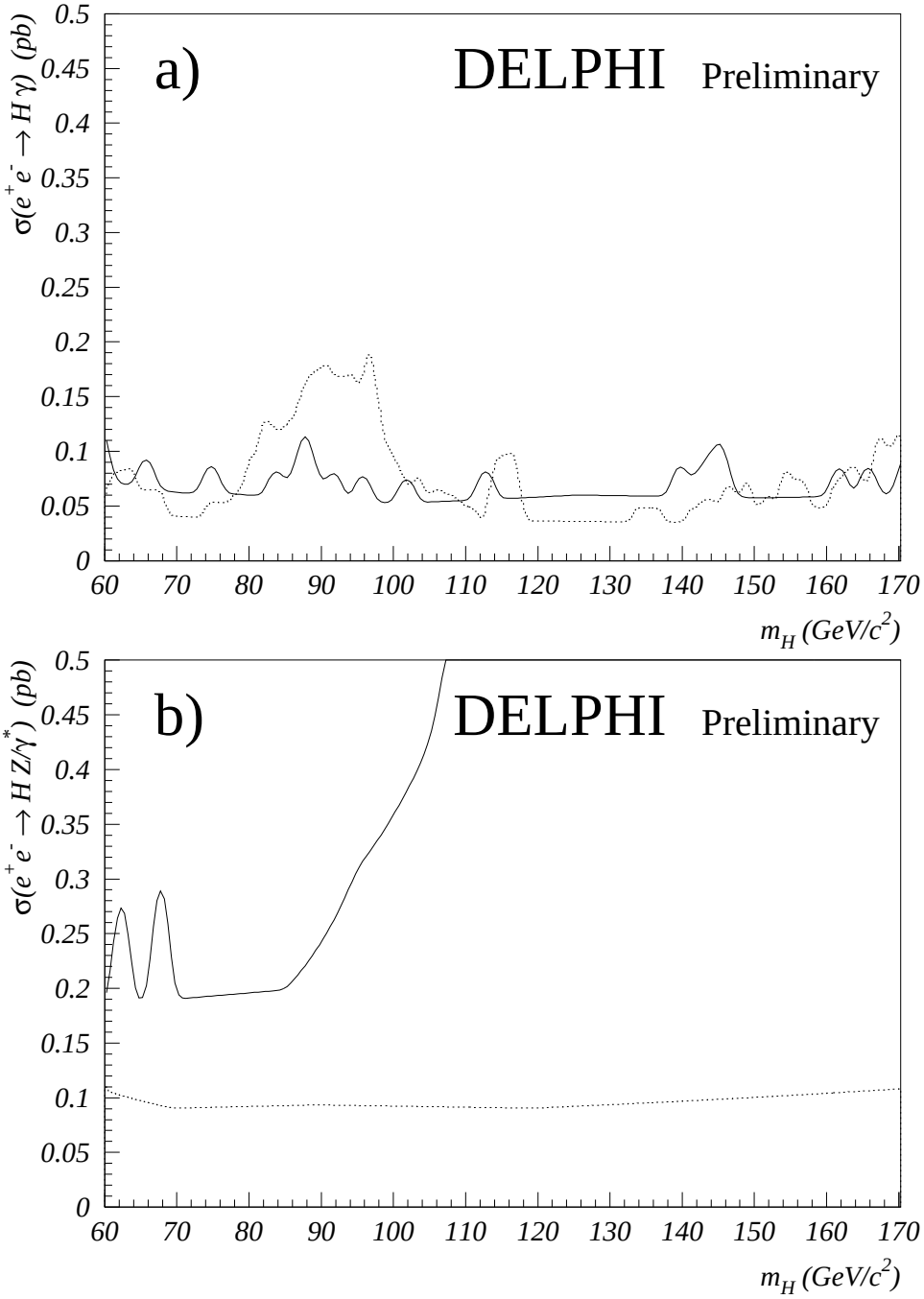

Figure 4: 95%CL upper limits on : a) $\sigma(e^+e^- \to H\gamma)$ with $H \to \gamma\gamma$ (full line) and $H \to b\bar{b}$ (dotted line) b) $\sigma(e^+e^- \to HZ/\gamma^*)$ with $H \to \gamma\gamma$ and $Z \to \nu\overline{\nu}$ (full line) and $Z \to q\bar{q}$ (dotted line).

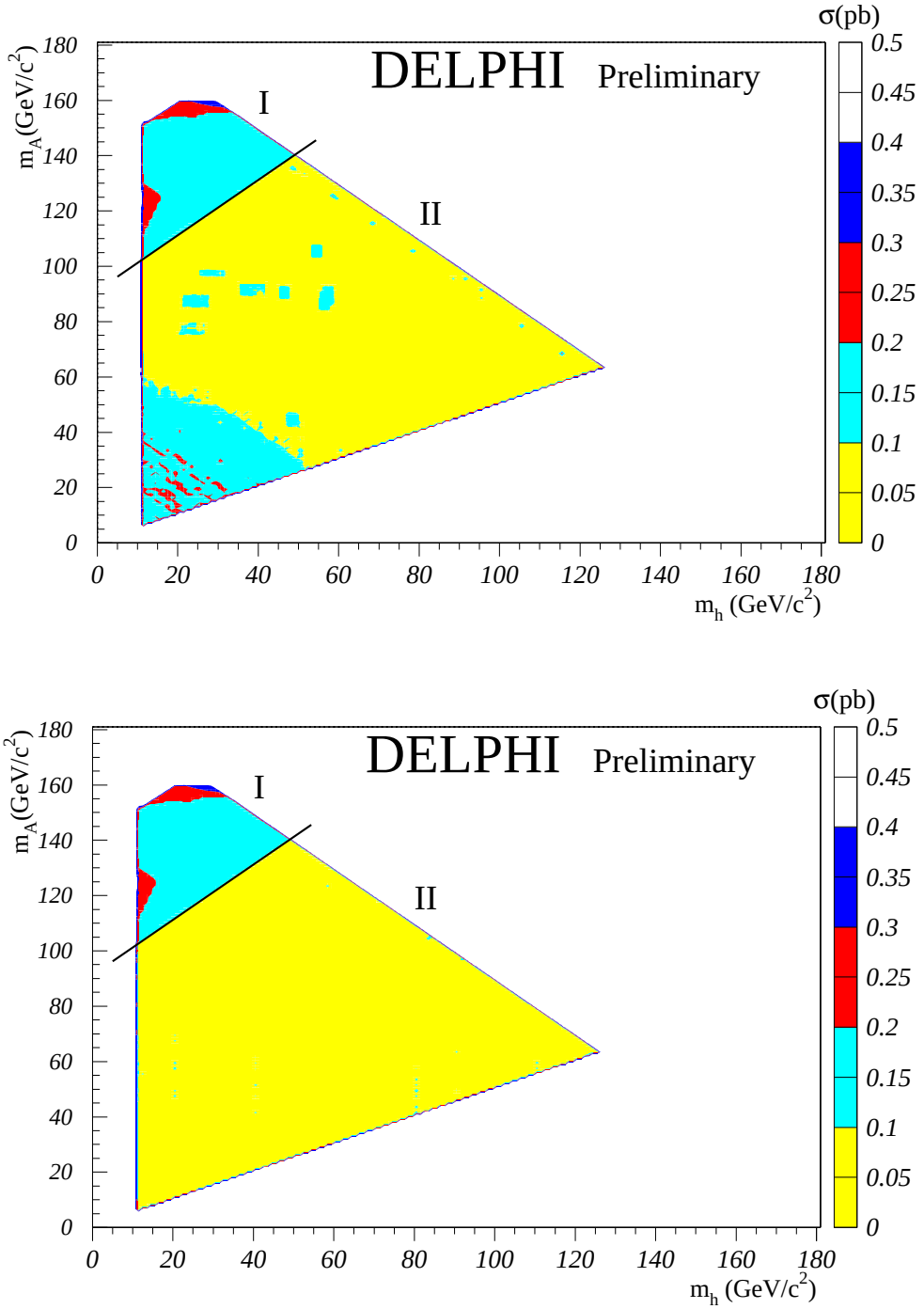

Figure 5: 95%CL upper limits on $\sigma(e^+e^- \to h^0A^0)$. In both plots the h^0 decays to $\gamma\gamma$ and region I corresponds to $A^0 \to h^0Z^0$. Region II corresponds to $A^0 \to b\bar{b}$ (upper plot) and A^0 long lived (lower plot). The decay modes in the upper plot are relevant for larger δ values ($\delta > 0.001$) and the ones in the lower plot for very small δ values

.

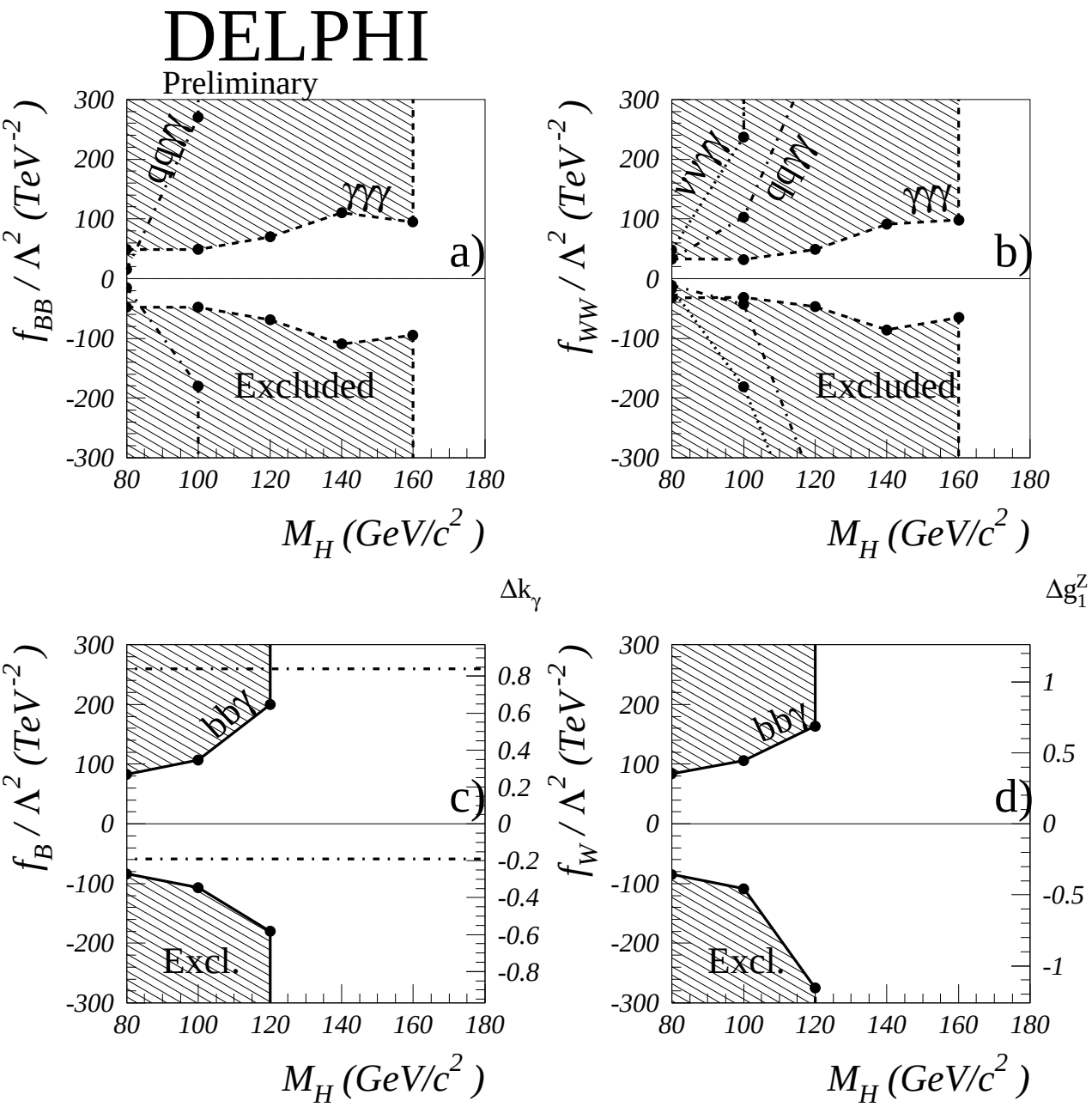

Figure 6: 95% CL limits on each f_i/Λ^2 parameter as a function of m_H, when all other f_i are set to zero. The full, dashed dotted and dashed-dotted lines correspond to the $b\bar{b}\gamma$, $\gamma\gamma\gamma$, $\nu\bar{\nu}\gamma\gamma$ and $q\bar{q}\gamma\gamma$ analysis, respectively. Only $b\bar{b}\gamma$ contributes to set limits on f_B and f_W. In c) and d) the right hand scales correspond to TGC parameters (Δk_γ and Δg_1^Z). The dashed-dotted line in c) is the 95% CL limit on Δk_γ from TGC measurements.

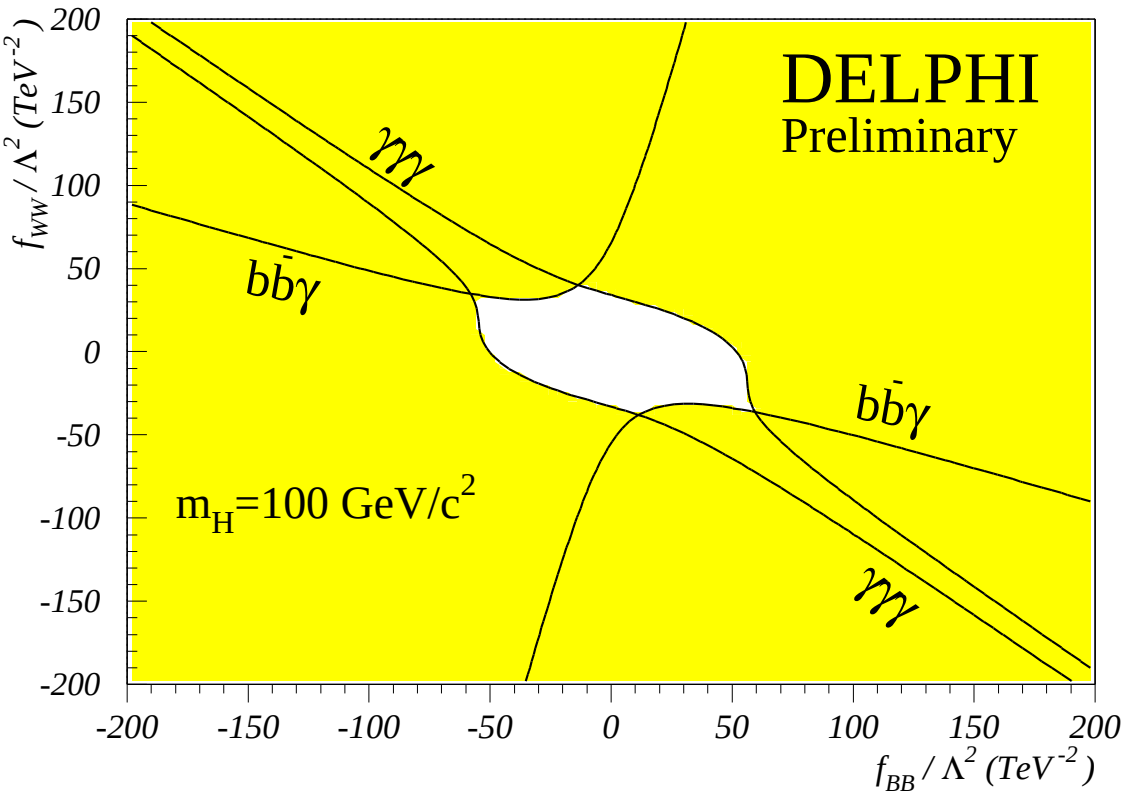

Figure 7: 95% CL exclusion regions in the $f_{BB} \times f_{WW}$ plane for $m_H = 100$ GeV/c^2. The contour lines correspond to the upper limits on the cross-section of the processes $b\bar{b}\gamma$ and $\gamma\gamma\gamma$. The shadowed regions are excluded.

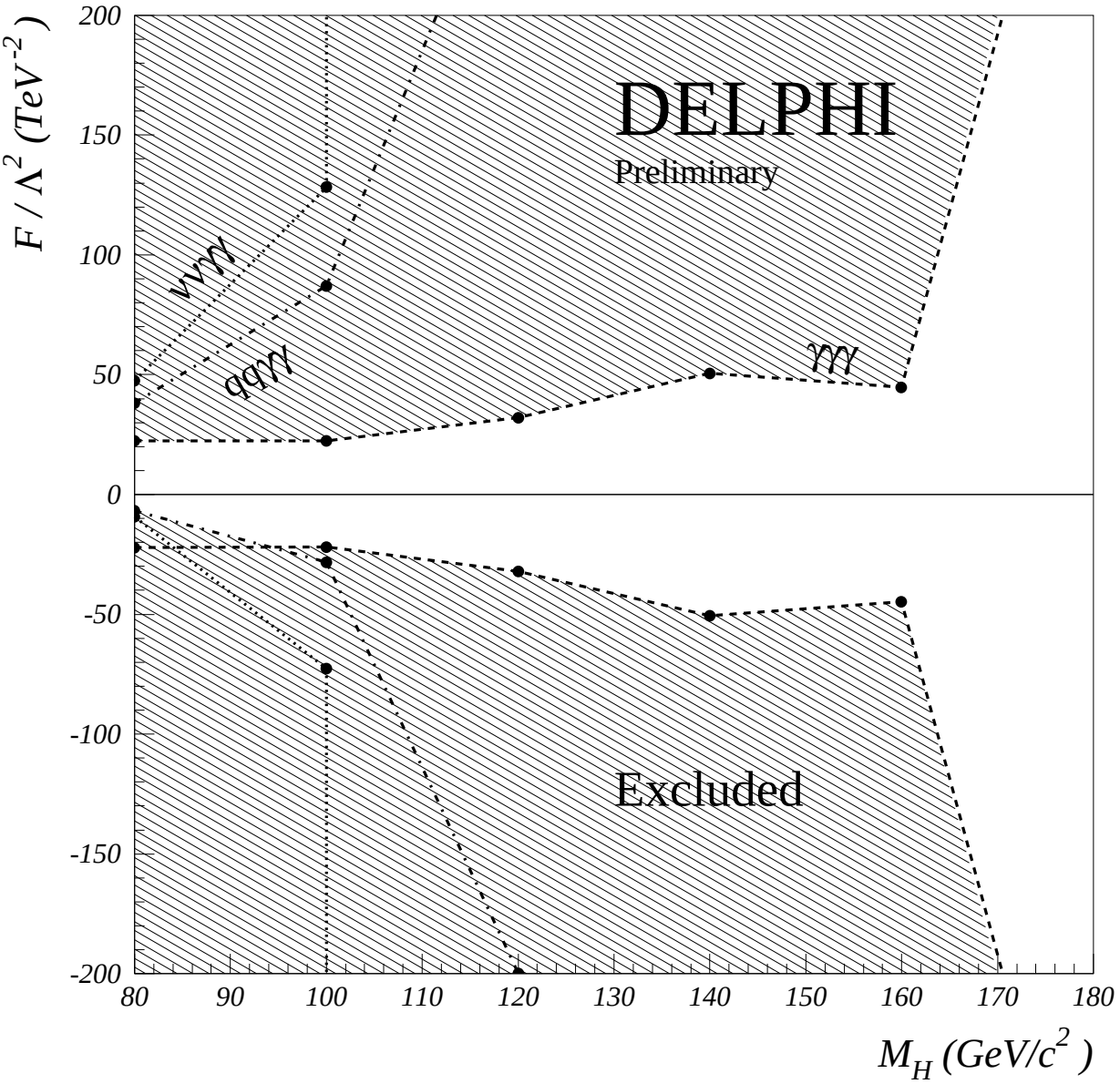

Figure 8: 95% CL limits on F/Λ^2 as a function of the Higgs boson mass. The dashed line corresponds to the $\gamma\gamma\gamma$, the dashed-dotted to the $q\bar{q}\gamma\gamma$ analysis and the dotted line to the $\nu\bar{\nu}\gamma\gamma$.

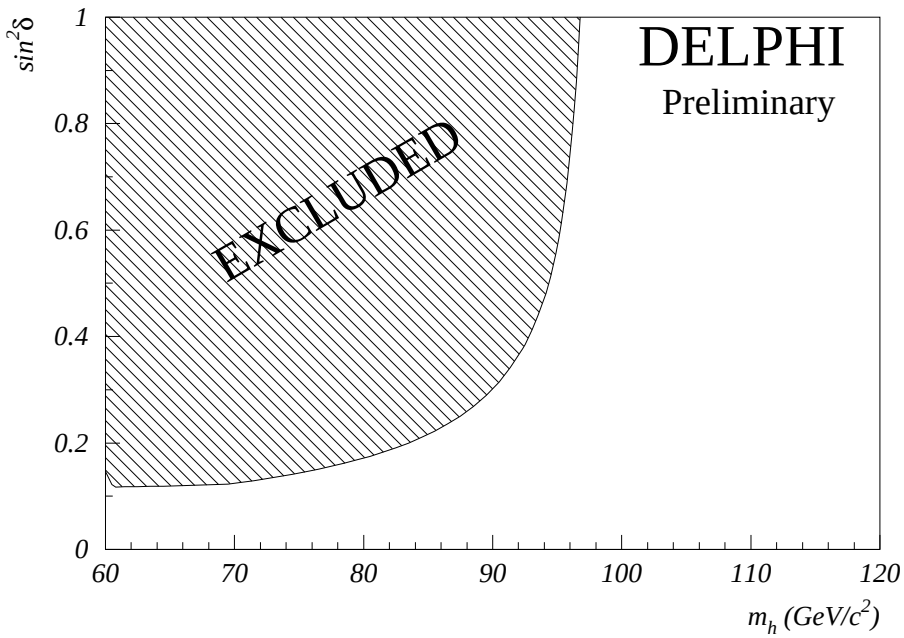

Figure 9: 95 % CL excluded region in the plane (m_{h^0}, $sin^2\delta$), obtained directly from the Higgs-strahlung final states, assuming $h^0 \to \gamma\gamma$.

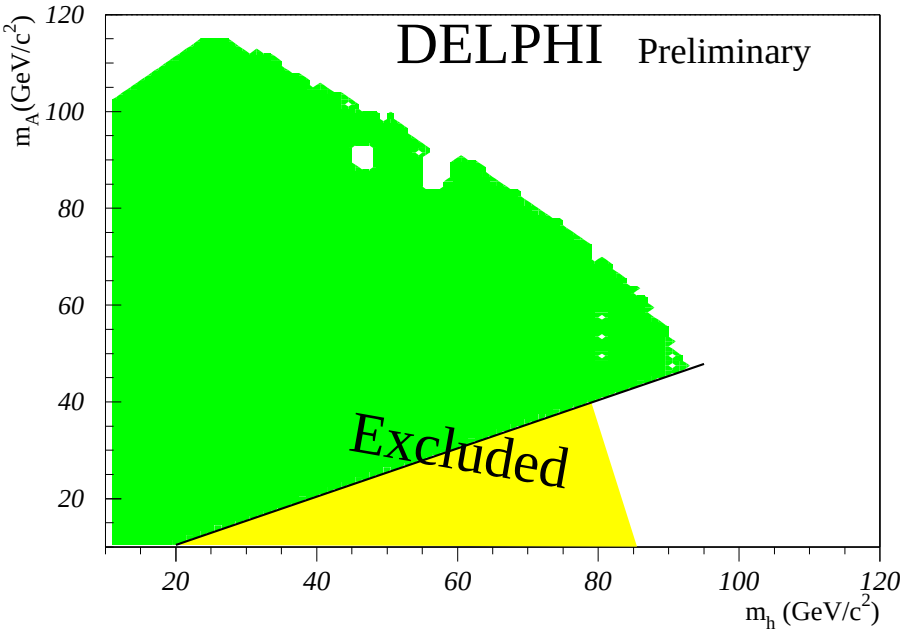

Figure 10: 95 % CL excluded region in the plane (m_{h^0},m_{A^0}), combining the Higgs-strahlung and the associated production process. The limits are valid for all δ values. The dark region corresponds to the decay modes $h^0 \to \gamma\gamma$ and $A^0 \to b\bar{b}$ or A^0 long-lived. The light region was taken from reference [22] and corresponds to $h^0 \to A^0A^0$ and $A^0 \to b\bar{b}$.